Seismic And Geomorphic Assessment For Coseismic Landslides Zonation In Tropical Volcanic Contexts

Mario Arroyo-Solórzano (mario.arroyosolorzano@ucr.ac.cr)
Universidad Politecnica de Madrid https://orcid.org/0000-0002-1653-2680
Adolfo Quesada-Román
Universidad de Costa Rica
Gustavo Barrantes-Castillo
Universidad Nacional de Costa Rica

Research Article

Keywords: coseismic landslides, susceptibility, Central America, Poás volcano, seismicity, tectonic geomorphology

Posted Date: February 4th, 2022

DOI: https://doi.org/10.21203/rs.3.rs-1321588/v1

Seismic and geomorphic assessment for coseismic landslides zonation in tropical volcanic contexts

Mario Arroyo-Solórzano [a,*], Adolfo Quesada-Román [b] and Gustavo Barrantes-Castillo [c]

[a] *Escuela Técnica Superior de Ingenieros en Topografía, Geodesia y Cartografía, Universidad Politécnica de Madrid, España.*

[b] *Escuela de Geografía, Universidad de Costa Rica.*

[c] *Escuela de Ciencias Geográficas, Universidad Nacional, Costa Rica.*

**Corresponding author*: Mario Arroyo-Solórzano (mario.arroyosolorzano@ucr.ac.cr).

Abstract

The Poás volcano is an active volcano of Costa Rica with intense tectonic activity in its flanks. Historically, the volcano has presented strong, surficial earthquakes provoking a large number of landslides with associated casualties and immense economic impacts. One example is the Cinchona earthquake in 2009 (Mw 6.2 and 4.6 km depth). We aim to determine a landslide zonation according to seismic data and a geomorphic assessment in the NW sector of the Poás volcano based on a combination of qualitative methods and morphometric parameters. The results estimated the possible outcome of a 6.8 Mw earthquake. The susceptibility mapping and models showed a positive relationship between this methodology and others previously developed for the area that surrounds the Poás volcano as well as a correspondence with the landslides caused by the Cinchona earthquake in 2009. The final zoning coseismic landslides susceptibility indicated that 52 % of the area is prone to landslides. Furthermore, there is a relationship between the areas with high exposure to landslides with conical volcanic geomorphologies, active faulting structural and/or tectonic geomorphological units with slopes greater than 15°. The proposed zoning can be useful in land use planning and by the responsible emergency entities to orientate quick response and reduce the impact of future landslides. Moreover, this method can be applied in active tectonic and volcanic areas worldwide.

Keywords: coseismic landslides; susceptibility; Central America; Poás volcano; seismicity; tectonic geomorphology

1. Introduction

One of the main natural hazards that seriously threaten the life and property of human beings are the landslides triggered by earthquakes (Kirschbaum et al. 2015; Lin et al. 2017). Central America is exposed to intense rainfall (3000-6000 mm/yr), weathering, hydrothermal alteration, erosion, and fluctuating temperatures typical of the tropics (Ruiz et al. 2019a). These conditions make this region vulnerable to multiple geohazards resulting from earthquakes, but mainly landslides (Bommer and Rodríguez 2002; Quesada-Román et al. 2019). In Costa Rica, there has been recurrent intermediate magnitude earthquakes near to volcanoes ($5.0 < M < 7.7$). Some of these have triggered destructive coseismic landslides during the last decades with an average rate of one damaging earthquake every three years (Climent et al. 2008; Linkimer et al. 2018). Compared to other regions of the world, Central America is known to have a disproportional and high number of landslides triggered by earthquakes (Keefer 1984; Rodríguez et al. 1999; Bommer and Rodríguez 2002; Ruiz et al. 2019a).

This landslide susceptibility is only comparable with some sectors of Southeast Asia and Oceania (Shi and Karsperson 2015). Some examples of comparable earthquakes are the 2011 Sikkim Mw 6.8 earthquake, the 2013 Lushan earthquake in Sichuan Ms 7.0 which caused 3883 landslides (Chen et al. 2020; Zhang et al. 2021) the 2015 Gorkha, Nepal Mw 7.8 earthquake which triggered more than 2064 landslides (Tian et al. 2019; Chen et al. 2020; Maharjan et al. 2021), and the relevant event of the 2008 Wenchuan, China Mw 7.9 earthquake which triggered more than 56,000 landslides (Dai et al. 2011; Li et al. 2020). Volcanos in Costa Rica are in an active tectonic setting with a high seismicity rate. In particular, the latest highly destructive event had a magnitude of 6.2 Mw Cinchona earthquake in 2009, which triggered approximately 4,600 landslides (Barrantes et al. 2013).

There are several methods to model landslide susceptibility. The approaches include the weight-of-evidence analyses, index-based, data-overlay, neural network analysis, linear multivariate regression, boosted regression tree analysis highlight, (e.g. Reichenbach et al. 2018; Arabameri et al. 2019; Chen et al. 2020; Li et al. 2020; Frigerio et al. 2021), discontinuous deformation analyses (DDA) (e.g., Chen et al. 2021; Zhang et al. 2021), remote sensing and high DEM resolution (e.g., Maharjan et al. 2021; Smail et al. 2021) and deep learning (e.g., Li et al. 2021). Two widely used landslide susceptibility methods in Latin America are the Mora-Vahrson-Mora (MVM) and the morphometric methods (Hengl and Reuter 2008; Barrantes et al. 2011; Quesada-Román and Barrantes 2016; Quesada-Román and

Barrantes 2017). The MVM method uses slope, lithological conditions, and humidity as control factors to susceptibility (Mora et al. 1992). In contrast, the morphometric method proposed by Quesada-Román and Barrantes (2017) uses the analysis of the slopes based on morphometric parameters such as depth and density dissection, relief energy, and total erosion, assigning weights and values for the susceptibility to occurrence of landslides. These are index-based or data overlap methods that allow the identification of areas with potential to manifest landslides and their triggers normally are heavy rains, earthquakes, or a combination of both. These methods have been used individually to evaluate landslide susceptibility in areas near Poás volcano and, in this paper, we propose a merge of some of its variables to propose a more robust and accessible hybrid method.

Researchers have studied the Cinchona earthquake and its subsequent landslides. First, a study using an airborne imagery mapped the landslides within the walls of the main active crater of Poás volcano and the geologic description of the area affected by landslides in route 126 at the eastern side of the Poás volcano (GVN 2009). In addition, a sedimentological analysis described the debris flows related to this seismic event, including a preliminary map of the landslides in the Poás massif (Alvarado 2010). Recently, other studies presented susceptibility models and landslides inventories (e.g., Barrantes et al. 2013; Quesada and Barrantes 2016; Ruiz et al. 2019a), and a national landslide risk index by municipality (Quesada-Román 2021). However, there is a lack of susceptibility evaluations as an integrated combination of complementary methods, which could help with interpretations in cases of limited information, especially for areas with scarce geological mapping.

We propose the evaluation of landslide susceptibility in the NW sector of the Poás volcano through the integration of the MVM method used by Ruiz et al. (2019a) and the morphometric parameters analysis. This research emphasizes coseismic landslides based on the evaluation of the seismic potential to propose the earthquake trigger for the modeling, looking for hypothetical large earthquakes. We seek to identify the worst-case scenarios that would generate landslides through a seismic analysis. Besides, we complement this with geomorphological mapping use to baseline for the final coseismic landslides zoning. It is intended to develop a landslide zoning that relates their greater or lesser incidence with the identified geomorphological units. Our approach can provide a reference for future disaster prevention, mitigation, and reconstruction zoning and a basis for landslide risk management in the NW sector of Poás volcano and/or other regions with analogous volcano-tectonic characteristics in tropical environments.

2. Study area

Costa Rica's Central Volcanic Arc was formed by the subduction of the Cocos plate under the Caribbean plate at relative plate movements of ~8 cm per year (DeMets et al. 2010). This subduction has resulted in active volcanism and the faulting of Quaternary stratovolcanoes (Marshall et al. 2000). Volcanic activity in current volcanic massifs began in the Late Cenozoic, and it currently consists of fumarole emissions and hot lakes within the craters (Fernandez 2013). This mountain range is a chain of andesitic stratovolcanoes oriented to the northwest, consisting of five main massifs: Platanar, Poás, Barva, Irazú, Turrialba, and several pyroclastic cones (Alvarado 2011).

The study area (Fig. 1) is located at the NW of the Poás volcano, within an active fault belt that has been called the Central Costa Rica Deformed Belt (CCRDB). Regional tectonic stress and/or volcanic processes control the neotectonic structures surrounding the volcanic massif. Around the Poás volcano, the Viejo-Aguas Zarcas, Sabanilla, El Angel and Carbonera faults are strike-slip faults-oriented NNW-SSE, while the San Miguel fault is a thrust fault with a general N70ºW orientation. Several authors mentioned that at least six historic shallow earthquakes of intermediate magnitude ($5.0 \leq M \leq 6.5$) have occurred near the Poás volcano in the last 242 years, which have generated destructive and deathly landslides in communities such as Sarchí, Grecia, Naranjo, Fraijanes, Bajos del Toro and Vara Blanca (Montero 2001; Montero et al. 2010; Ruiz et al. 2014; Montero 2014).

This area mainly comprises the upper basin of the Toro River, which drains toward the Caribbean basin. The limit was defined according to the available geological information (Ruiz et al. 2019b) and represents the west sector of the area covered by LiDAR data and high-resolution orthophotos after the Cinchona earthquake in 2009. A small proportion that is not covered by the LiDAR images has been complemented based on data from information of the BID-cadaster program with a resolution of 10 m in the Z axis (Epypsa 2011). The study area covers part of the mesoseismic area where the landslides triggered by the Cinchona earthquake occurred, the NW flank of the Poás volcano and part of the NE flank of the Platanar volcano. Most of the land use is covered by protected forest use; however, there are some important population settlements and agricultural sectors. In addition, there are important hydroelectric dams for electricity production in the country, and it is also a key touristic important touristic area of Costa Rica, with one of the top visited national parks: the Poás volcano National Park (Fig. 1).

The most important geological formations of the Poás volcano are the units Paleo Barva, Volcán Platanar, Andesites La Paz, Achiote, Lavas Río Cuarto, and the Volcán Poás Summit, composed mainly of andesitic-basaltic lava, lahars, ignimbritic and pyroclastic deposits (Fig. 2). These geological formations, their lithology, age, and evolution are described by Alvarado et al. (2011) and Ruiz et al. (2019b) and have been used in this paper as reference to explore the influence of the lithology and the geological units age, with the susceptibility to present landslides. This effect has been previously described by Ruiz et al. (2019a), which associate higher susceptibility to older geological units.

3. Data and methods

3.1. Geomorphological mapping

We developed a geomorphological map at 1:25,000 scale to help understand the genesis, morphology, and chronology of the landscape of the NW of the Poás volcano and relate it to the analyses of the main seismic sources and finally with the proner landslides zones. First, three digital elevation models (DEM) and a terrain analysis were created to obtain more detail of the geomorphological units. One of these DEMs have a resolution of 10m, obtained from cadastral information (Epypsa 2011), the other one has a 20 m resolution, obtained from aerial photos of the 2005 CARTA project, and the last one is from LiDAR images, obtained from the Costa Rican Institute of Electricity (ICE), with three points per m^2 and the resulting DEM presents a resolution of 50 cm on the X and Y axes, and 15 cm on the Z axis. We analyzed the terrain models and chose the LiDAR imagery model to define the geomorphological units. These LiDAR images were acquired between March and April 2009.

The terrain models allow the interpretation of detailed local geomorphological units, defined mainly by means of slopes, geometry, and river drainage network analyses, and using, as reference, the regional geomorphology of the Geomorphological Atlas of Costa Rica at a scale of 1:100,000 (Bergoeing and Brenes 2017). Finally, the landform, its geometry, morphometry, and its relation to the geological and tectonic context was interpreted to map the genesis, dynamics, morphology, and evolution of the different landforms and its processes using various digital graphic techniques to develop the final cartographic product (Gustavsson et al. 2006; Bishop et al. 2012; Otto et al. 2018). The resulting landforms were classified into fluvial, gravitational, structural, and volcanic genesis.

3.2. Seismic analysis

The maximum earthquake magnitude (Mmax) is defined as the largest possible earthquake for a seismogenic zone or region (e.g., Kijko 2004). The seismic sources were identified firstly based on previous neotectonics studies (Denyer et al. 2003; Montero et al. 2010) from which we selected the Viejo-Aguas Zarcas, Carbonera, Sabanilla, Ángel, and San Miguel as the faults that represent the greatest threat to the study area. Then, the historical and instrumental seismicity of these faults were inspected according to the location of epicenters, magnitudes, and depth of the earthquakes. In addition, we inspected the traces of the tectonic structures and faults from aerial photographs and LiDAR data and two epicenters were chosen which asserts possible worst scenarios in the fault traces near to the interest area.

For the Mmax approximation, we used the seismic zoning proposed by Alvarado et al. (2017), specifically the crustal seismic zone of the Central Volcanic Range and the Costa Rica's Central Valley (C6). Based on the seismological catalog of the National Seismological Network of Costa Rica (RSN) (Arroyo-Solózano & Linkimer 2021; Red Sismológica Nacional de Costa Rica 2021), between 1975-2020, and the portion of the historical catalog from Rojas et al. (1993), between 1723-1975, we used the Gutenberg-Richter (1944) recurrence law ($\log N = a - bM$), in which N is the number of earthquakes greater or equal to magnitude M, and the a and b values are constants. The seismicity was modeled using a homogeneous catalog in Mw, the minimum magnitude was set to 3.0, the completeness analysis was taken according to the results from Arroyo et al. (2017) and using the Gardner and Knopoff (1974) declustering method. We based this analysis on 7825 seismic events from 1 to 40 km depth, determining the seismic parameters a and b-values by the Weichert (1980) maximum likelihood approximation. Moreover, we based the Mmax on the Makropoulos and Burton (1983) method, which is a pseudo-graphic formulation that approximates the Mmax by transforming the accumulated amount of the seismic moment into magnitude (e.g., Weatherill 2014). This approach was executed using the Hazard Modeler Toolkit (Weatherill 2014) of the OpenQuake software (GEM 2020).

We also evaluated the mean recurrence interval (MRI) of magnitudes above 5.0 Mw for the seismic zone C6. This is usually the time to elapse between two subsequent earthquakes of a given magnitude rupturing on a given seismogenic source (e.g., Wang 2007; Salazar 2018). This can be described by the Gutenberg-Richter relationship, if M is solved in terms of the frequency of the events (1/t) based on the estimated a and b-values. Besides, we estimated the

accumulated probability of occurrence exceedance (POE) of the Mmax earthquake observed and inferred in the analysis for this seismic source, based on Poisson's theory, defined as $P(t) = 1-e^{-\lambda t}$ (Cárdenas et al. 2010; Rivas et al. 2014). This is approximated from the annual exceedance probability, which is very similar to λ (annual exceedance rate of earthquakes of a given magnitude). When graphing the Gutenberg-Richter relationship in terms of the earthquake frequency, λ is equal to N, obtaining $N = 10^{a-b*M}$, getting the accumulated probability of occurrence for the magnitude of interest and evaluating these results for different periods.

3.3. Landslide susceptibility modeling

The model proposed by Ruiz et al. (2019a) is based on the MVM model (Mora and Vahrson 1991 and 1993; Mora et al. 1992). This approach considers four control factors elements: 1) Lithological susceptibility (Sl), 2) Slope susceptibility (Sp), 3) Humidity content susceptibility (Sh) and 4) the landslide trigger event (DT), which uses the attenuation of the Peak Ground Acceleration (PGA) produced by an earthquake. This model has the advantage of specializing in earthquakes as landslide triggering events, and it can be applied to different shallow earthquakes with different characteristics in location, depth, and magnitude. Likewise, Quesada and Barrantes (2017), based on morphometric parameters, used the dissection density (d), the dissection depth (p), the relief energy (E), and the total erosion (ET) to assess landslide susceptibility (SPL).

We propose to use the Ruiz's model as a base but incorporating the morphometric parameters (M): dissection density (d) and dissection depth (p), replacing the lithological susceptibility parameter (Sl). This substitution has been defined to avoid giving a double weight to lithology since both the dissection and density and dissection depth have been observed in previous studies as closely related to the lithology of the geological units and their ages. Also, this is suggested since the access to the drainage network and topographic models are commonly easier to obtain than geological detailed information in some areas. Equation 1 shows the resulting integration for the landslide susceptibility (SPL) proposed:

$$SPL = (\mathrm{Sp} * \mathrm{Sh} * M) * \mathrm{DT} \qquad (1)$$

Where: $M = (d + p)/2$

3.3.1. Control factors

194 Landslide susceptibility comprises multiple factors. The quantity and accuracy of the control factors determine the
195 quality of landslide susceptibility maps (Tien et al., 2016). We chose the slope, humidity content, and morphometric
196 parameters as the most significant. To assess the slope susceptibility (Sp) (Fig. 3a), the generation of a digital terrain
197 elevation model (DEM), explained in section 3.1, and its subsequent calculation of slopes were required. The slope
198 classes are based on expert criteria from the MVM method, which define seven slope classes (0; 0.1-4º; 4-8º; 8 -16º;
199 16-35º; 35-55º and > 55º), assigning a weight between 0 and 6, with 0 being the least susceptible and 6 the most
200 susceptible.
201
202 For the humidity content susceptibility (Sh) (Fig. 3b), the original estimation is obtained from a water balance based
203 on monthly precipitation records. We propose to vary the calculation of this factor using the humidity provinces
204 (Herrera 1985), specifically their water indices assigning weights from 1 to 5 as follow based on expert criteria and
205 following the assigning weights logic of the MVM method: 1=0%; 2=0-20%; 3=20-100%, 4=100-300% and 5=300-
206 600%). This percentage relates the mean annual precipitation (mm) (P) and the annual potential evapotranspiration
207 (ETP), as Im=(P/ETP-1) *100. These provinces are based on weather types for Costa Rica, determined by annual
208 water balances, representing a mean of the humidity conditions. These kinds of indices are useful in areas where
209 baseline information and meteorological stations are scarce and to consider altitude's influence in the humidity
210 regimen.
211
212 To include the morphometric parameters (M) (Fig. 3c), the rivers were first identified from the DEM obtained by
213 LiDAR (section 3.1). Subsequently, the area was divided into quadrants with individual surfaces of 0.1 km^2, the
214 centroid of each of these was obtained, and its respective ID assigned. The dissection density (d) was calculated
215 obtaining the concentration of rivers per unit area while the dissection depth (p) is explained as the height difference
216 between the talweg and the maximum height of the analyzed quadrant. Consequently, the values for each quadrant
217 were interpolated using the Kriging method, and a classified into five classes by the statistical method of quantiles.
218 To combine the two morphometric variables (M) the range of values obtained for both depth and dissection density
219 were normalized between 0 and 1 (Oyana 2021) and combined by means of the multiplication by a map algebra
220 process. Finally, five classes are established using quantiles classification. This represents the selected morphometric

parameter (M), being consistent with the other susceptibility parameters established by Mora and Vahrson (1991 and 1993), being 1 the least susceptible and 5 the most susceptible.

3.3.2. Trigger landslide event

The seismic trigger (DT) is determined from the evaluation of the seismic potential and hypothetical earthquakes. These earthquake scenarios were modeled as simple fault by means of the *Input Preparation Toolkit* of the OpenQuake platform (GEM 2020) according to the epicenters of the hypothetical scenarios obtained from the analyses of the seismic potential explained in section 3.2. The modeling of deterministic scenarios in OpenQuake by means of this toolkit, allows to estimate the PGA values by means of the earthquake rupture definition: coordinates, magnitude, depth, and rake of the hypothetical earthquake and dip, upper, and lower depth of the fault source. Then, the Vs30 values of the soils is added to incorporate the site effects in the calculation. We used the Global Vs30 Mosaic of the United States Geological Survey (USGS), based on topographic slope, with custom embedded maps (Heath et al. 2020) and classified it in the soils classes according to the NEHRP (2020) classification. Finally, the PGA values were computed in OpenQuake engine, using a rupture mesh spacing of 0.2 km, a grid region spacing of 1 km and the Ground Model Prediction Equation (GMPE) of Zhao et al. (2006). This GMPE was selected according to Benito et al (2012), who conclude this as one of the equations that fit better with the attenuation observations for Central America's crustal earthquakes.

Once the PGA values were obtained, they are converted to a weight between 1-7 according to the MVM method. For this process, we took the PGA values obtained from OpenQuake engine for each point on the grid of the study area and transformed it to the weight ranges for the trigger factor, described before. This was carried out by means of an empirical formula with a better logarithmic fit, proposed by Ruiz et al. (2019a): DT=1,2597* ln (PGA)-1,2517.

3.3.3. Susceptibility maps and landslide zonation

According to the hypothetical earthquakes, based on a worse-case scenario and selected according to the procedures explained in section 3.1, the different values of each control and trigger factors (sections 3.3.1 and 3.3.2) were integrated by means of a map algebra, obtained by the multiplication of each of them. Then, they were classified into

248 five classes, by means of equal intervals, and the susceptibility to coseismic landslides was obtained. The classes used
249 were very high, high, moderate, low, and very low.
250
251 To verify the effectiveness of the modeling, the Cinchona 2009 earthquake was additionally modeled follow the same
252 methodology proposed for the hypothetical earthquakes, as a real case of comparison and model validation of the
253 susceptibility classes. It was also modeled by means of OpenQuake engine as simple fault, based on El Angel Fault
254 trace and according to its earthquake location and the rupture parameters based on Barquero (2009): 6.2 Mw, 4.6 km
255 depth, rake -36.86°, dip 47.3° and upper and lower seismic depth of 0 and 15 km, respectively.
256
257 We combined previous landslide catalogs (Barrantes et al., 2013; Ruiz et al., 2019a), which correspond to the
258 Cinchona earthquake. Each of these catalogs contain more than 4000 landslides, but we just evaluated the landslides
259 in the eastern sector of the study area (available landslides information), using the Rio Toro as reference. This landslide
260 catalog was revised according to the aerial photos from the Carta 2005 project and the slopes were selected where
261 landslides occurred, eliminating the deposits of them. This approach draws the interest in this study, evaluate zones
262 where landslides could occur, not slip volumes or slip deposit zones. Also, some landslides were repeated in both
263 catalogs, so a revision and selection of them was necessary to avoid duplications. The resulting catalog consists of
264 606 landslides and a total slip area of 2.37 km^2. The verification was made by means of relationships between
265 landslides areas and susceptibility areas obtained by the model using the Cinchona earthquake as trigger.
266
267 Finally, to represent the landslide susceptibility zoning, the susceptibility maps were averaged by means of a map
268 algebra processing. This was done to obtain a global view of the susceptibility for the entire area, that contemplate the
269 possibility of a big earthquake, both, north and south of the study zone. The result was classified into three classes:
270 high, moderate, and low using Natural breaks classification (Jiang, 2013), to simplify the final global analysis and
271 seeking to group the previous classes of very high and high, and the classes of very low and low susceptibility.
272
273 **4. Results**
274 **4.1. Geomorphological units**
275 *Linkime4.1.1. Endogenic landforms*

Tectonic-structural and depositional volcanic forms represent endogenic landforms controlled mainly by the volcano-tectonic fracture of the Poás volcano (Fig. 4). The most relevant structural morphology identified corresponds to the fault scarp (E1) of the San Miguel Fault, located in the northern sector. The most prominent expression is a scarp 100 to 300 m high, which extends 15 km and even affects the drainage of the Sarapiquí River. Upstream of the fault scarp, the deep canyons are antecedents of this tectonic structure, which has its maximum height in the central part, decreasing towards the east and west. There are also a series of paleo-landslides along the scarp.

As volcanic morphologies, we determined the following: Caldera (V1), Volcanic crater (V2), Maar (V3), Secondary volcanic cones (V4), Flow fields and pyroclastic deposits (V5), and low (V6), moderate (V7) and high (V8) volcanic slopes. The volcanic crater (V2) is the active crater of the Poás Volcano, the Maares (V3) are Laguna Hule and Río Cuarto. The latter has been determined to be a gasmaar based upon the concentrations of CO_2 that accumulates deep in the lagoon. The secondary volcanic cones (V4) are Cerro Congo and Von Frantzius, which responded to old sources of emissions and are not currently active. The pyroclastic flow fields and deposits (V5) are associated with areas modeled by this type of recent activity with ash deposits from the Poás Volcano. Finally, the volcanic slopes reflect the mountainous relief produced by the volcanic deposits. The low slope (V6) responds mainly to more distant deposits and products of lahars or pyroclastic flows while those moderate (V7) and high (V8) slope make up the volcanic buildings of Poás and Platanar, made up mainly of lava and pyroclastic deposits.

4.1.2. Exogenic landforms

Exogenic landforms are constituted by erosive and depositional landforms of fluvial and gravitational origin (Fig. 4). The fluvial genesis forms (F) respond directly to the action of the rivers, especially the Río Toro and some of its main tributaries. Two fluvial morphologies are identified, the floodplain (F1) of the Río Toro in the central sector and to the SW and the river canyons (F2) that cross the mountainous sector. The floodplains correspond to the settlement areas of some of the main towns of Bajos del Toro. The origin of these floodplains is due to river sectors that have not yet down-cut enough through the geological substrate enough to overcome the depositional processes that occur during flooding. The river canyons have depths between 50 and 100 m deep and are located mainly to the NW, the main one is the Río Toro canyon.

304 We also determined three gravitational morphologies: the erosion slopes (G1), the colluvial deposit (G2), and
305 landslides scarps remnant (G3). These morphologies mostly respond to erosion processes on steep slopes and the
306 accumulation of these deposits in flat or horizontal sectors. The erosion slopes, or foothills (G1), are mainly related to
307 areas such as hills at the foot of the volcanic slopes, which have been shaped by erosive processes. Colluvial deposits
308 (G2) are accumulation zones close to rivers and erosion slopes. Finally, ancient landslide zones (G3) respond to large
309 landslides that have generated a specific geomorphology; these landslides are related to the Congo and Von Frantzius
310 secondary volcanic cones.
311
312 **4.2. Seismicity and seismic potential**
313 Six important historical earthquakes have affected the study area. Three of these of 6.0 Mw occurred in 1772-02-15,
314 1888-12-30, and 1911-08-28, one of 5.5 Mw in 1912-06-06, one more of 6.1 Mw in 1955-09-01 in the Viejo-Aguas
315 Zarcas fault and the Cinchona earthquake on 2009-01-09 (6.2 Mw) (Fig. 5a). Based on these historic earthquakes and
316 according to the location of the epicenters, zones near faults that have not presented big ruptures yet and the trace
317 faults analyses, we follow the deterministic criterion in terms of locating the epicenter within or as close as possible
318 to the study area (worst scenarios) to select the trigger earthquakes (Fig. 5a). Scenario 1 consists of locating the
319 epicenter at the Viejo-Aguas Zarcas fault, within the study area, related to Viejo-Aguas Zarcas fault. The second
320 scenario proposes to locate it where an earthquake could occur in the San Miguel Fault, assuming a dip of ~30° for
321 this fault, in the NW sector of Cerro Congo. The highest Mmax determined is 6.8 Mw and the shallow depth 5 km,
322 based on the depth distribution of the earthquakes into the C6 seismic zone, with great influence of the Central Costa
323 Rica Deform Belt (Fig. 5b).
324
325 The recurrent law parameters (a and b-values) estimated for C6 were 3.59 and 0.82, respectively, and the inferred and
326 observed Mmax (Mw) were 6.4 and 6.8, respectively. The magnitude frequency distribution observed in these
327 parameters suggests that the MRI in seismic zone C6 for the observed Mmax (6.4 Mw) is ~70 years and for the
328 inferred Mmax (6.8 Mw) it is ~110 years (Fig. 6a). The POE was also estimated for the observed and inferred Mmax,
329 which resulted in a probability of occurrence greater than 80% for the observed Mmax (6.4 Mw) in ~75 years and for
330 the inferred Mmax (6.8 Mw) in ~155 years (Fig. 6b).
331

4.3. Susceptibility maps

Control factors (Fig. 3) showed for Sp the highest weights (3, 4, 5 and 6) correspond to scarps and river canyons, as well as mountain slopes and erosive cuts of the Poás and Platanar volcanoes, and low weights (1, 2) are mainly associated with plains and foothills. For Sh, the results showed three humidity provinces: humid, very humid, and excessively humid, with weights of 3, 4 and 5, respectively. This shows differences between mountainous areas of higher altitude in the Poás and Platanar volcanoes, with respect to flat areas and in the Toro River valley. In the case of M, areas of lower weight (1) are associated with low slopes (<15°), those of moderate weight (2 and 3) to the foothills, and those of greater weight (4 and 5) are associated to volcanic slopes, as well as the deep canyons of the Toro River.

The Vs30 values for the study area shows a direct influence of the topography, with a range between 900 and 245 m/s, and classified in soils B, CB, C and D of the NEHRP (2020) classification (Fig. 7a). The derived site effect is observed in the PGA maps (Figs. 7b y 7c), it highlights the effect of high acceleration around the fault trace and the lower Vs30 values correlated with less attenuation of the seismic movement. Scenario 1 earthquake rupture was computed assuming a strike slip fault movement with a rake angle of 0° and a Dip angle of 90° (Fig. 7b). Scenario 2 earthquake rupture was computed assuming a trust fault movement, with a rake angle of 90°, and a Dip angle of 30° (Fig. 7c). For both hypothetical earthquake scenarios the magnitude was defined as 6.8 Mw, a depth of 5 km, and an upper and lower seismogenic zone of 0 and 15 km, respectively. The results of the acceleration distribution show that PGA values greater than 500 cm/s^2 could occur in a radius of ~10 km, close to the selected epicenters, with maximum intensities expected for both earthquakes of up to IX on the Modified Mercalli Intensity scale (MMI) (Fig. 7b and 7c).

The DT values and the susceptibility maps obtained for each of the hypothetical scenarios are shown in Fig. 8a and 8b. For scenario 1, the distribution according to the modeling of susceptibility to landslide was very low = 36.1 %, low = 27.8 %, moderate = 22.7 %, high = 12.1 % and very high = 1.3 %. The areas classified as high or very high susceptibility are located near the epicenter, specifically in the steep slope zone without vegetation located west of the main Poás crater, as well as on the southeast flank of the Platanar Volcano and the Toro River canyons (Fig. 8a). For scenario 2, the distribution of the susceptibility categories is as follows: for very low susceptibility 31.8 %, low = 28.8 % =, moderate = 23.4 %, high = 13.3 % and very high = 2.7 % (Fig. 8b).

360

361 **4.4. Susceptibility model validation**

362 The Cinchona earthquake landslide catalog (described in section 3.3.3) was used to verify the model (Fig. 9a). We
363 evaluated the total slipped area percentage, the relationship between the slipped area by susceptibility category and
364 the category area (Fig. 9). Table 1 shows the distribution of landslides and part of the statistical and percentage data,
365 with respect to the susceptibility categories, obtained according to the final landslides catalog. The zones with the
366 greatest slipped area were high, moderate, and very high susceptibility categories. The relationship between the slipped
367 area and the area of the susceptibility category allows us to determine the percentage of the area of each category that
368 slides (Table 1 and Fig. 9b and 9c). Fig. 9b shows very small landslide areas in low and very low susceptibility, mainly
369 corresponding to sectors with low slope and distances far from the epicenter.

370

371 There is also a proportional increase in the slipped area as the susceptibility category rises, with a greater amount of
372 slipped area in the high and very high susceptibility categories. Fig. 9c and Table 1 show that large areas of very low
373 susceptibility have, in proportion to their size, a very low percentage of landslide area (less than 1%) whereas the areas
374 in the very high susceptibility category, in relation to its relatively small area, approximately 20% of its area exhibited
375 landslides. The frequency of landslides showed in Table 1 also shows that more landslides were in moderate, high,
376 and very high susceptibility, compared to low and very low, despite the fact that these last categories present much
377 more area, which also supports the model effectivity to identify prone areas.

378

379 **4.5. Landslides susceptibility zonation**

380 Fig. 10 shows three zones of high, moderate, and low hazard to coseismic landslides. These were defined by selecting
381 the classification that best encompasses the modeled scenarios in a consistent manner. Low hazard zones (48 %) are
382 associated with slopes less than 20°, where the occurrence of significant landslides is not expected. Moderate hazard
383 zones (35 %) are characterized by slopes that generally exceed 20°, in sectors of the upper and middle basin of the
384 Río Toro. The high hazard zones (17 %) are distributed near the upper catchments areas, in sectors of higher altitude
385 and that are characterized by steep slopes (> 30°). The foregoing is associated with pyroclastic ramps, canyoning river,
386 and the slopes of the Poás and Platanar volcanic complexes. This allows the development of landslides, mudflows,
387 and complex movements.

5. Discussion

5.1. Methodological and model implications

The seismic and geomorphological assessment determined that the faults with the greatest seismic potential are the San Miguel, Viejo-Aguas Zarcas, Sabanilla and Carbonera fault. Some studies proposed the Venecia fault (Barquero 2009; however, in this investigation, according to Montero et al. (2010) and the geomorphological mapping, we interpreted it as a continuation of the El Angel Fault towards the NW (Fig. 2, 4 and 5a). The possible existence of a fault in the canyon of the Toro River would also be important, nevertheless, there is not enough evidence to confirm its existence. We also identified and mapped a Caldera (V1) (Fig. 4) which had been previously reported in the Tectonic Atlas of Costa Rica (Denyer et al., 2003). Bergoeing and Brenes (2017) suggested that the Platanar-Porvenir Volcano could be part of a large collapsed caldera of up to 36 km in diameter, which highlights the importance of the hypothetical epicenter in the Viejo-Agua Zarcas fault.

The Mmax estimated was a 6.8 Mw, similar to the seismic potential associated to the C6 seismic zone and its faults in other studies (6.7-7.0 Mw) (Climent et al. 2006; Climent et al. 2008; Alvarado et al. 2017; Arroyo 2019, Arroyo-Solórzano and Linkimer 2021). The earthquake scenarios modeled has been defined based on the fault trace strike, modeling it as a simple fault, assuming a centroid moment tensor in the epicenter selected as a trigger point. This exhaustive selection of scenarios and the rupture modeled reflect the most probable natural behavior, with maximum PGA values along the faults trace. We consider that this source proximity effect has a very significant influence in the values obtained, and they are very important to be considered in the seismic hazard approaches. However, this effect is not always determinant because it has been identified that large-scale landslides could occur in areas with low PGA, and not always high PGA zones present landslides, an example was observed during the 2016 Kumamoto earthquake (Chen et al. 2021).

The highest probability of occurrence for the earthquakes modeled is ~ 95% over 500 years. This model covers the most probable scenarios such as the observed Mmax of 6.4 Mw (Fig. 6). The approximation method used assumes that no earthquakes are occurring at the corresponding time. Furthermore, there is no consideration of other processes that contribute to the energy release in an aseismic way such as post-seismic deformation. Despite the possibility that

416 the method overestimates Mmax, it is widely used because provides the upper limit of the seismic potential based on
417 observed magnitudes.
418
419 The susceptibility maps have some key factors that improve the estimation from the previous MVM method. First, the
420 Sh modification allows to differentiate humidity content susceptibility in different parts of the basin. This factor varies
421 according to biotemperature and evapotranspiration. In high-altitude and mountainous areas, it is usually lower than
422 low-altitude and flat areas. This condition favors a higher humidity content in the high-altitude areas, assigning greater
423 Sh weight to the susceptibility of landslides in these sectors. It is important to indicate that this factor changes during
424 the year due to the heavy raining season, but it works as an average annual value of humidity. Second, the
425 morphometric parameters (M), respond to the presence of faults and fractures as well as to lithology, specifically the
426 Paleo Poás Units (800-200 ka), which exhibit strong weathering, favoring the dissection depth and density. This allows
427 to determine morphometric parameters that could substitute in a good way the geological maps in zones with scarce
428 geology information. Finally, in the seismic analyses we incorporated the seismic catalog recurrence evaluation, which
429 was not applied in previous studies. Additionally, for the PGA expected values, the local effects of seismic
430 amplification were also incorporated, based on Vs30 topographic values from (Heath et al. 2020). It is very important
431 to consider this as a key factor for landslides susceptibility. We propose to improve this site effect map (Fig. 7a) with
432 field geotechnical measures for a better characterization of the soils.
433
434 The susceptibility model shows an accurate and effective simulation (Fig. 9b and 9c). Despite categories of low and
435 very low susceptibility present large areas, the slides zones were mostly in very high, high and moderate susceptibility
436 areas. According to Mora et al. (1992), landslides could occur in areas of moderate, high, and very high susceptibility.
437 Based on this, 52 % of the study area is prone to present landslides (moderate and high susceptibility zones, Fig. 10)
438 and only the low-angle slopes would be safe. However, low susceptibility sectors with deep river valleys could develop
439 mudflows/lahars due to the presence of weathered lavas and juvenile or recent pyroclastic deposits. If earthquakes
440 such as those modeled occur, it could create a dangerous situation due to landslides triggered, even in areas located
441 more than 15 km from the epicenter. For both hypothetical events, the geological units of the Paleo-Poás or Platanar
442 Volcano temporal phase show greater susceptibility, which agrees with the observations of Ruiz et al. (2019a).
443

444 **5.2. Geomorphic and seismological approach for coseismic landslides hazard zonation**

445 The baseline of the methodology developed follows the MVM method and its modifications over time (Mora et al.
446 1993; Ruiz et al. 2019a). This method is similar to the logic applied in other studies worldwide (e.g., Tian et al. 2018;
447 Shao et al. 2019; Chen et al. 2020). Other studies (Xu et al. 2013; Fan et al. 2018; Li et al. 2020; Li et al. 2021) have
448 carried out an inverse process, evaluating based on the catalog of landslides, the higher incidence of these events and
449 determining the possible trace of the fault responsible for the earthquake. This methodology is more useful for areas
450 with little knowledge of local tectonics or to complement seismic source analyses. In volcanic and tropical
451 environments such as the Poás volcano, both methods are feasible and effective in overcoming the difficulty of
452 tracking surface fault rupture in the field due to dense vegetation. This limitation in tropical volcanic environments
453 could be solved using unmanned aerial vehicles, even low-cost ones (Granados-Bolaños et al. 2021) and by means of
454 radar satellite images and remote sensing new technologies (Maharjan et al. 2021; Smail et al. 2021).
455
456 Many studies (e.g., van Westen et al. 2006; Fell et al. 2008; Gorum et al. 2013; Morell et al. 2018; Chunga et al. 2019;
457 Chen et al. 2020) concluded that the integration of geomorphic and seismic data of sufficient quantity and quality into
458 seismic hazard approaches greatly improves coseismic landslides hazard models. Our model improves previous MVM
459 and morphometric models since it integrates and complements both types of methodologies and assigns a weight
460 categorization according to the original MVM model. This is because geomorphological and seismic data has been
461 exhaustively analyzed for the definition of the trigger, and some control factors have been adapted to obtain better
462 detail (as with Sh) and substituting others to make the evaluation more accessible (as with M). Multiple studies also
463 indicated that a precise geomorphic assessment, morphometric data, humidity, soils, and detailed seismological data
464 improve the prediction of events in tropical-volcanic environments (e.g., Dai et al. 2011; Lin et al. 2017; Otto et al.
465 2018; Fan et al. 2018; Ruiz et al. 2019a; Li et al. 2020; Arabameri et al. 2019; Tian et al. 2019; Chen et al. 2020;
466 Maharjan et al. 2021; Smail et al. 2021; Zhang et al. 2021).
467
468 The main contribution of the proposed methodology is the detailed evaluation of the seismicity. This is accomplished
469 through a seismological probabilistic analysis from the seismic catalog to determine the Mmax and complemented by
470 means of a deterministic analysis based on earthquake scenarios obtained from the seismotectonic analyses and
471 seismic potential assessment. This aspect is highly relevant since it has been used in studies such Xu et al. (2013),

Morell et al. (2018), Shao et al. (2019), Chen et al (2021) and Zhang et al. (2021) who evaluate the effects in areas with respect to the seismogenic fault, and its intensity is crucial for spatial prediction of intensities and coseismic landslides. Our results show that the method is accurate for use in landslide susceptibility zoning and applicable to land use planning. We also consider that the greatest susceptibility for settlements and road infrastructure would be the transformation of these landslides into lahars, which was also mentioned by Ruiz et al. (2014).

Finally, we considered that the tropical context and the topography of volcanic environments such as in the NW Poás volcano provide a significant opportunity to keep working in developing methods to characterize the behavior of earthquake-trigger landslides in these sectors in a better way, and to compare this with other contexts. An example of this is shown by Ruiz et al. (2019a), where the magnitude of landslides from the Cinchona earthquake were compared with another earthquake with similar characteristics in California, USA. They found a great difference in the number of landslides and a clear difference in the aforementioned factors, showing more coseismic landslides in tropic-volcanic environments.

6. Conclusions

Based on the integration of the modified Mora Vahrson Mora (MVM) and morphometric methods, as well as the geomorphological and seismicity analysis, landslide susceptibility maps were determined for the NW sector of the Poás volcano in Costa Rica. Control factors were adapted, two of these being derivatives of the MVM (slope angle (Sp) and humidity content (Sh)), and two taken from the methodologies that evaluate morphometric parameters (density and depth dissection (M)). Moreover, the earthquake trigger (DT) was added based on the geomorphic and seismic analysis. Therefore, worst-case earthquake scenarios are proposed as two hypothetical earthquakes. The 2009 Cinchona earthquake was also modeled as an earthquake scenario and their susceptibility categories were validated through the landslide catalog of this earthquake, showing a very good fit between landslides and the more susceptible categories. Then, the two scenarios were integrated and a susceptibility zoning map to coseismic landslides was obtained.

Our results improved the local knowledge due to the control factor detail implemented in the model. More precise and detailed information was obtained using the Sp and M factors by the digital elevation model based on the LiDAR

images, as well as the Sh, by means of a water index. In addition, 14 local geomorphological units have been mapped to show differences between endogenic and exogenic landforms and considered for the seismotectonic analyses and the selection of the location of the epicenters in the earthquake scenarios. Furthermore, the seismic potential (Mmax) results in a 6.8 Mw and a depth of 5 km for the hypothetical earthquakes. These earthquakes have been modeled: one with an epicenter associated with the Viejo-Aguas Zarcas fault (scenario 1) and the other with the San Miguel fault (scenario 2). The validation of the method with the 2009 Cinchona earthquake showed an adequate correspondence between categories and real landslides with most of the landslides found in the moderate, high and very high susceptibility categories predicted by our model. The susceptibility zoning map to coseismic landslides indicated that 52 % of the area has a high probability of landslides. Conical volcanic landforms and those on slopes greater than 15° are the most prone to landslides, being the slope the most relevant control factor.

The results also serve as the basis for generating similar studies in other parts not only of Costa Rica, but of the world, in volcanic and seismically active regions with limited geological data. The main virtues of the proposed method are the improved detail in some control factors and the use of easily obtainable morphometric parameters to replace lithology, as well as the integration of a geomorphic and seismic analysis. The methodology is recommended as an input for risk mitigation and territorial planning and based on these models and a computational development, early warning systems (EWS) can be implemented in real time to help prioritize sources of attention to disasters. It is also recommended to integrate these results with probabilistic landslides hazard models in the future and complement this with the assessment of landslides triggered by heavy rains. Coseismic landslide susceptibility zonation is the first step to integrate the different elements at risk such as the hazard, exposition, and vulnerability.

Acknowledgments

This research was carried out thanks to the support provided with the grants system for dissertations works from the National High Technology Center (CeNAT) and the PRIAS Laboratory. We thank the personnel of the CeNAT, special thanks to Christian Vargas, Andres Barahona and Daniel Flores (PRIAS-CENAT) for their observations provided in earlier stages of this research. Special thanks to Dr. Pablo Ruiz for his valuable collaboration, suggestions and corrections that highly improved the manuscript. In addition, we are grateful with Russell Lee Losco and Soll Kracher for the English grammar revision.

528

529 **References**

530 Alvarado GE (2010) Aspectos Geohidrológicos y sedimentológicos de los flujos de lodo asociados al terremoto de
531 Cinchona (Mw 6,2) Del 8 de enero del 2009, Costa Rica. Revista Geológica de América Central, 43, 67-96

532 Alvarado GE (2011) Los volcanes de Costa Rica: Geología, historia y riqueza natural. San José: 3a ed. EUNED.

533 Alvarado GE, Benito B, Staller A, Climent Á, Camacho E, Rojas W, Lindholm C (2017) The new Central American
534 seismic hazard zonation: Mutual consensus based on up to day seismotectonic framework. Tectonophysics,
535 721, 462–476. http://dx.doi.org/10.1016/j.tecto.2017.10.013.

536 Alvarado GE, Soto GJ, Salani FM, Ruiz P, Hurtado L (2011) The formation and evolution of Hule and Río Cuarto
537 maars, Costa Rica. Journal of Volcanology and Geothermal Research, 201, 342–356.
538 https://doi.org/10.1016/j.jvolgeores.2010.12.017

539 Arabameri A, Pradhan B, Rezaei K, et al. (2019) GIS-based landslide susceptibility mapping using numerical risk
540 factor bivariate model and its ensemble with linear multivariate regression and boosted regression tree
541 algorithms. Journal of Mountain Science 16(3): 595-618. https://doi.org/10.1007/s11629-018-5168-y

542 Arroyo M (2019) El parámetro sísmico b de la Relación Gutenberg-Richter en Costa Rica. -126 págs. Dissertation,
543 Universidad de Costa Rica, San José, Costa Rica.

544 Arroyo M, Godínez K, Linkimer L (2017) Completitud del catálogo de la Red Sismológica Nacional de Costa Rica
545 durante 1975-2014. Boletín de Geología, 39(3), 87-98.

546 Arroyo-Solórzano M, Linkimer L (2021) Spatial variability of the b-value and seismic potential in Costa Rica.
547 Tectonophysics, 814 (2021) 228951. https://doi.org/10.1016/j.tecto.2021.228951

548 Barquero R (2009) El terremoto de Cinchona del 8 de enero de 2009. San José, Costa Rica: RSN.

549 Barrantes G, Barrantes O, Núñez O (2011) Efectividad De La Metodología Mora-Vahrson Modificada En El Caso De
550 Deslizamientos Provocados Por El Terremoto De Cinchona, Costa Rica. . Revista Geográfica de América
551 Central., 47, 141–162.

552 Barrantes G, Jiménez C, Ocón M (2013) Deslizamientos provocados por el terremoto de Cinchona de 2009, Costa
553 Rica. Revista Geográfica de América Central, (51): 89–100.

554 Barrantes G, Salcedo E (2016) Consideración de la amenaza sísmica en el Ordenamiento Territorial del cantón de
555 Poás, Costa Rica. Boletín de Geología, 38(3): 109-127.

556 Benito B, Lindohlm C, Camacho E, Climent A, Marroquin G, Molina E, Rojas W, Escobar J, Talavera E, Alvarado
557 GE, Torres Y (2012) A New Evaluation of Seismic Hazard for the Central America Region. Bulletin of the
558 Seismological Society of America. Vol. 102 (2): 504–523.
559 Bergoeing JP, Brenes LG (2017) Atlas Geomorfologico de Costa Rica: Escala 1: 100000. Primera Edicion. Escala
560 1:100000. Heredia, Costa Rica. EUNA, 2017. 72 págs.
561 Bishop M., James A, Shroder J, Walsh SJ (2012) Geospatial technologies and digital geomorphological mapping:
562 Concepts, issues, and research. Geomorphology, 137, 5–26. https://doi.org/10.1016/j.geomorph.2011.06.027
563 Bommer JJ, Rodríguez CE (2002) Earthquake-induced landslides in Central America. Engineering Geology 63, 189-
564 220.
565 Cárdenas C, Garzón Y, Santa L, Castillo L (2010) Modelo de Poisson para la ocurrencia y magnitud espacio-temporal
566 de los sismos en Colombia. UD y la Geomática. 4: 28-43.
567 Chen G, Xia M, Thuy DT, Zhang Y (2021) A possible mechanism of earthquake-induced landslides focusing on pulse-
568 like ground motions. Landslides, 18(5), 1641-1657. https://doi.org/10.1007/s10346-020-01597-y
569 Chen L, Mei L, Zeng B, Yin K, Shrestha DP, Du J (2020) Failure probability assessment of landslides triggered by
570 earthquakes and rainfall: a case study in Yadong County, Tibet, China. Sci Rep 10, 16531 (2020).
571 https://doi.org/10.1038/s41598-020-73727-4
572 Chunga K, Livio FA, Martillo C, Lara-Saavedra H, Ferrario MF, Zevallos I, Michetti AM (2019) Landslides Triggered
573 by the 2016 Mw 7.8 Pedernales, Ecuador Earthquake: Correlations with ESI-07 Intensity, Lithology, Slope
574 and PGA-h. Geosciences 9, 371. https://doi.org/10.3390/geosciences9090371
575 Climent A, Alvarado GE, Boschini I (2006) PH Toro 3: estudio de amenaza sísmica. San José, Costa Rica: Instituto
576 costarricense de electricidad (ICE).
577 Climent A, Rojas W, Alvarado GE, Benito, B (2008) Proyecto Resis II, Evaluación de la amenaza sísmica en Costa
578 Rica. San José, Costa Rica: Upm, NORSAR.
579 Dai FC, Xu, C, Yao X., et al. (2011) Spatial distribution of landslides triggered by the 2008 Ms 8.0 Wenchuan
580 earthquake, China. Journal of Asian Earth Sciences 40(4): 883-895. https://doi.org/10.1016
581 /j.jseaes.2010.04.010.
582 Denyer P, Montero W, Alvarado GE (2003) Atlas Tectónico de Costa Rica. San José, Costa Rica: Universidad de
583 Costa Rica.

584 DeMets C, Gordon RG, Argus DF (2010) Geologically current plate motions. Geophys. J. Int. 181, 1–80.
585 http://dx.doi.org/10.1111/j.1365-246X.2009.04491.x.
586 Epypsa (2011) Informe final de Consultoría Elaboración de planes reguladores costeros. Programa de Regularización
587 de Catastro y Registro. San José, Costa Rica.
588 Fan X, Scaringi G, Xu Q, Zhan W, Dai L, Li Y, Pei X, Yang Q, Huang R (2018) Coseismic landslides triggered by
589 the 8th August 2017 Ms 7.0 Jiuzhaigou earthquake (Sichuan, China): factors controlling their spatial
590 distribution and implications for the seismogenic blind fault identification. Landslides 15, 967–983.
591 https://doi.org/10.1007/s10346-018-0960-x
592 Fell R, Corominas J, Bonnard C, Cascini L, Leroi E, Savage W (2008) Guidelines for landslide susceptibility, hazard
593 and risk zoning for land-use planning. Engineering Geology. 102, 99–11.
594 https://doi.org/10.1016/j.enggeo.2008.03.014
595 Fernandez M (2013) Seismotectonic and the Hipothetical Strike – Slip Tectonic Boundary of Central Costa Rica.
596 Earthquake Research and Analysis - New Advances in Seismology, 77-105.
597 Frigerio Porta G, Bebbington M, Xiao X, Jones G (2021) A Statistical Model for Earthquake And/Or Rainfall
598 Triggered Landslides. Front. Earth Sci. 8:605003. doi: 10.3389/feart.2020.605003
599 Gardner JK, Knopoff I (1974) Is the sequence of earthquakes in Southern California, with aftershocks removed,
600 Poissonian?, Bulletin of the Seismological Society of America, 64(5), 1363–1367.
601 GEM (2020) The OpenQuake-engine User Manual. Global Earthquake Model (GEM) OpenQuake Manual for Engine
602 version 3.9.0. doi: 10.13117/GEM.OPENQUAKE.MAN.ENGINE.3.9.0, 183 pages.
603 Granados-Bolaños S, Quesada-Román A, Alvarado GE (2021) Low-cost UAV applications in dynamic tropical
604 volcanic landforms. Journal of Volcanology and Geothermal Research, 410, 107143.
605 https://doi.org/10.1016/j.jvolgeores.2020.107143
606 Gustavsson M, Kolstrup E, Seijmonsbergen AC (2006) A new symbol-and-GIS based detailed geomorphological
607 mapping system: Renewal of a scientific discipline for understanding landscape development.
608 Geomorphology, 77(1–2), 90–111. https://doi.org/10.1016/j.geomorph.2006.01.026
609 Gutenberg B, Richter C (1944) Frequency of earthquakes in California. Bulletin of the Seismological Society of
610 America, 34, 185-188.

611 GVN (2009) Fatalities from a large earthquake; slide and minor eruption in crater. Smithsonian Institution. BGVN
612 34:01.
613 Heath D, Wald DJ, Worden CB, Thompson EM, Scmocyk G (2020) A Global Hybrid VS30 Map with a Topographic-
614 Slope-Based Default and Regional Map Insets", Earthquake Spectra, vol. 36, 3: pp. 1570-1584.
615 Hengl T, Reuter HI (Eds.) (2008) Geomorphometry: concepts, software, applications. Newnes.
616 Herrera W (1985) Clima de Costa Rica. Vegetación y clima de Costa Rica. Vol 2. EUNED. San Jose, Costa Rica.
617 Jiang B (2013) Head/tail breaks: A new classification scheme for data with a heavy-tailed distribution. The
618 Professional Geographer, 65(3), 482-494.
619 Keefer DK (1984) Landslides caused by earthquakes. Geological Society of America Bulletin 95, 406-421.
620 Kijko A (2004) Estimation of the Maximum Earthquake Magnitude, MMAX. Pure and Applied Geophysics 161, 1655
621 –1681.
622 Kirschbaum D, Stanley T, Zhou Y (2015) Spatial and temporal analysis of a global landslide catalog. Geomorphology
623 249:4-15.
624 Li N, Tang C, Yang T, et al. (2020) Analyzing post-earthquake landslide susceptibility using multi-temporal landslide
625 inventories — a case study in Miansi Town of China. Journal of Mountain Science 17(2).
626 https://doi.org/10.1007/s11629-019-5681-7
627 Li Y, Cui P, Ye C, Junior JM, Zhang Z, Guo J, Li J (2021) Accurate Prediction of Earthquake-Induced Landslides
628 Based on Deep Learning Considering Landslide Source Area. Remote Sens., 13, 3436.
629 https://doi.org/10.3390/rs13173436
630 Lin L, Lin Q, Wang Y (2017) Landslide susceptibility mapping on a global scale using the method of logistic
631 regression. Natural Hazards and Earth System Science 17(8):1411-1424.
632 Linkimer L, Arroyo IG, Alvarado GE., Arroyo M, Bakkar H. (2018). The National Seismological Network of Costa
633 Rica (RSN): An Overview and Recent Developments. Seismological Research Letters, 89 (2A), 392-398.
634 Maharjan S, Gnyawali KR, Tannant DD, Xu C, Lacroix P. (2021). Rapid Terrain Assessment for Earthquake-
635 Triggered Landslide Susceptibility with High-Resolution DEM and Critical Acceleration. Front. Earth Sci.
636 9:689303. doi: 10.3389/feart.2021.689303
637 Makropoulos K, Burton P (1983) Seismic Risk of Circum-Pacific Earthquakes I. Strain Energy Release. Pure and
638 Applied Geophysics 121.2, pages 247 –266.

639 Marshall JS, Fisher DM, Gardner TW (2000) Central Costa Rica deformed belt: Kinematics of diffuse faulting across
640 the western Panama block, Tectonics, 19, 468-492.
641 Montero W (2001) Neotectónica de la región central de Costa Rica. Revista Geológica de América Central, 29-56.
642 Montero W (2014) Neotectónica en la Revista Geológica de América Central. Revista Geológica de América Central,
643 Número Especial 2014: 30 Aniversario: 83-98.
644 Montero W, Soto G, Alvarado GE, Rojas W (2010) División del deslizamiento tectónico y transtensión en el macizo
645 del volcán Poás (Costa Rica), basado en estudios neotectónicos y sismicidad histórica. Revista Geológica de
646 América Central, 13-36.
647 Mora S, Vahrson W (1991) Determinación a priori de la amenaza de deslizamientos sobre grandes áreas, utilizando
648 indicadores morfodinámicos. Memoria sobre el Primer Simposio., (págs. 259-273). Bogotá, Colombia.
649 Mora R, Mora S, Vahrson, W (1992) Microzonificación de la amenaza de deslizamientos y resultados obtenidos en el
650 área del valle central de Costa Rica. Escala 1:286 000 Ceprenac, San José Costa Rica.
651 Mora S, Vahrson W (1993) Determinación "a priori" de la amenaza de deslizamientos utilizando indicadores
652 morfodinámicos. Tecnología ICE, (3): 1-32.
653 NEHRP (2020) Recommended Provisions for seismic Regulations for New buildings and other Structures, Part 1:
654 Provisions, FEMA 368, Federal Emergency Management Agency, Washington, D.C.
655 Otto JC, Prasicek G, Blöthe J, Schrott L (2018) GIS Applications in Geomorphology. Comprehensive Geographic
656 Information Systems. Elsevier Inc. https://doi.org/10.1016/B978-0-12-409548-9.10029-6
657 Oyana TJ (2021) Spatial Analysis with R: Statistics, Visualization, and Computational Methods. CRC Press.
658 Quesada-Román A, Barrantes G. (2016) Procesos de ladera cosísmicos del terremoto de Cinchona (Costa Rica) del 8
659 de enero de 2009 (Ms=6,2). Cuadernos de Geografía: Revista Colombiana de Geografía, 25 (1): 217-232.
660 DOI: 10.15446/rcdg.v25n1.52590.
661 Quesada-Román A, Barrantes, G (2017) Modelo morfométrico para determinar áreas susceptibles a procesos de
662 ladera. Investigaciones Geográficas.
663 Quesada-Román A, Fallas-López B, Hernández-Espinoza K, Stoffel M, Ballesteros-Cánovas JA (2019) Relationships
664 between earthquakes, hurricanes, and landslides in Costa Rica. Landslides 16(8):1539-1550.
665 https://doi.org/10.1007/s10346-019-01209-4

Quesada-Román A (2021) Landslide risk index map at the municipal scale for Costa Rica. International Journal of Disaster Risk Reduction, 56, 102144. https://doi.org/10.1016/j.ijdrr.2021.102144

Red Sismológica Nacional de Costa Rica (2021) The Costa Rica National Seismological Network Catalog during 1975-2020. DOI: https://doi.org/10.15517/TC

Reichenbach P, Rossi M, Malamud BD, et al. (2018) A review of statistically based landslide susceptibility models. Earth- Science Reviews 180: 60-91. https://doi.org/10.1016/j.earscirev.2018. 03.001

Rivas A, Aguiar R, Benito B, Gaspar J, Parra, H (2014) Determinación del período de recurrencia y magnitud máxima para el control de las estructuras en el rango elástico ante un sismo asociado a las fallas inversas de Quito. Revista Internacional de Ingenieria y Estructuras, 19,2, 203 - 221.

Rodríguez CE, Bommer JJ, Chandler RJ (1999) Earthquake-induced landslides: 1980-1997. Soil Dynamics and Earthquake Engineering 18, 325-346.

Rojas W, Cowan H, Lindholm C, Dahle A, Bungum H (1993) Regional Seismic Zonation for Central América a Preliminary Model. 40 pp. Norsar Report: Norway.

Ruiz P, Carr M, Alvarado GE, Soto G, Mana S, Feigenson M, Sáenz, L (2019a) Coseismic Landslide Susceptibility Analysis Using LiDAR Data PGA Attenuation and GIS: The Case of Poás Volcano, Costa Rica, Central America. In: Tassi F., Vaselli O., Mora Amador R. (eds) Poás Volcano. Active Volcanoes of the World. Springer, Cham. https://doi.org/10.1007/978-3-319-02156-0_4.

Ruiz P, Mana S, Gazel E, Soto GJ, Carr MJ, Alvarado GE (2019b) Geochemical and Geochronological Characterisation of the Poas Stratovolcano Stratigraphy. In: Tassi F., Vaselli O., Mora Amador R. (eds) Poás Volcano. Active Volcanoes of the World. Springer, Cham. https://doi.org/10.1007/978-3-319-02156-0_2

Ruiz P, Soto G, and Barrantes R (2014) Uso de imágenes LIDAR en el estudio de la vulnerabilidad de la red vial Nacional, caso de estudio Ruta N°126. Congreso de Ingenieria Civil CIC 2014, (pág. 18). San José, Costa Rica.

Salazar W (2018) Principles of probabilistic seismic hazard assessment (PSHA) and site effect evaluation and its application for the volcanic environment in El Salvador. V. Svalova (Ed.), Earthquakes: Forecast, Prognosis and Earthquake Resistant Construction, doi: 10.5772/intechopen.75845.

Shao X, Chong X, Siyuan M, Qing Z (2019) Effects of Seismogenic Faults on the Predictive Mapping of Probability to Earthquake-Triggered Landslides. ISPRS Int. J. Geo-Inf. 8, no. 8: 328. https://doi.org/10.3390/ijgi8080328

694 Shi P, Karsperson R (eds.) (2015) World atlas of natural disaster risk. Heidelberg: Springer.

695 Smail T, Abed M, Mebarki A, Lazecky M (2021) Earthquake-induced landslides monitoring and survey by means of
696 InSAR, Nat. Hazards Earth Syst. Sci. Discuss. [preprint], https://doi.org/10.5194/nhess-2021-208, in review.
697 Tian Y, Chong Xu, Haoyuan H, Qing Z, Wang D (2019) Mapping earthquake-triggered landslide susceptibility by
698 use of artificial neural network (ANN) models: an example of the 2013 Minxian (China) Mw 5.9 event,
699 Geomatics, Natural Hazards and Risk, 10:1, 1-25. doi: 10.1080/19475705.2018.1487471
700 Tien Bui D, Tuan TA, Klempe H, Pradhan B, Revhaug I (2016) Spatial prediction models for shallow landslide
701 hazards: a comparative assessment of the efficacy of support vector machines, artificial neural networks,
702 kernel logistic regression, and logistic model tree. Landslides. 13(2):361–378.
703 Gorum T, van Westen CJ, Korup O, van der Meijde M, Fan XM, van der Meer FD (2013) Complex rupture mechanism
704 and topography control symmetry of mass-wasting pattern, 2010 Haiti earthquake. Geomorphology, 184,
705 127–138. https://doi.org/10.1016/j.geomorph.2012.11.027
706 van Westen C, van Asch T, Soeters R (2006) Landslide hazard and risk zonation—why is it still so difficult? Bull
707 Eng Geol Environ 65, 167–184. https://doi.org/10.1007/s10064-005-0023-0
708 Wang Z (2007) Seismic hazard and risk assessment in the intraplate environment: The New Madrid seismic zone of
709 the central United States. In Stein, S. and Mazzotti, S. ed., Continental Intraplate Earthquakes: Science,
710 Hazard, and Policy Issues. Geological Society of America Special Paper 425, 363–373,
711 doi:10.1130/2007.2425(24).
712 Weatherill G (2014) OpenQuake Hazard Modeller's Toolkit. User Guide. Global Earth-quake Model (GEM).
713 Technical Report.
714 Weichert D (1980) Estimation of the Earthquake Recurrence Parameters for Unequal Observation Periods for
715 Different Magnitudes. Bulletin of the Seismological Society of America, 70.4, 1337 - 1346.
716 Xu C, Xu X, Zhou B, Yu, G. (2013), Revisions of the M 8.0 Wenchuan earthquake seismic intensity map based on
717 co-seismic landslide abundance. Natural Hazards, 69, 1459–1476. https://doi.org/10.1007/s11069-013-0757-
718 0
719 Zhang, X, Xie B, Wang H, Jiao Y (2021) Study on the Dynamic Response of Landslide Subjected to Earthquake by
720 the Improved DDA Method. Modelling and Simulation in Engineering, vol. 2021, Article ID 6637939, 11
721 pages. https://doi.org/10.1155/2021/6637939

Zhao JX, Zhang A, Asano Y, Ohno T, Oouchi T, Takahashi H, Ogawa K, Irikura HK, Somerville PG (2006) Attenuation relations of strong ground motion in Japan using site classification based on predominant period, Bull. Seismol. Soc. Am.96, 898–913.

Statements and Declarations

Data availability

Some or all data, models, or code that support the findings of this study are available from the corresponding author upon reasonable request.

Author contributions

Mario Arroyo-Solórzano designed the study and wrote the paper with contributions from Adolfo Quesada-Román. All the authors interpreted and analyzed the results and revised the article.

Competing interests

There are no competing or financial interests to disclose.

739 **Table 1**. Landslides distribution based on susceptibility category in the eastern sector of the study area.

740

Susceptibility category	Susceptibility category area (eastern sector)		Landslides area		Landslides area km^2/susceptibility category area	Landslides frequency	
	km2	%	km^2	%	km^2	No.	%
Very high	2.20	1.70	0.65	27.43	0.295	85	14.03
High	12.95	9.96	1.00	42.19	0.077	198	32.67
Moderate	27.70	21.31	0.58	24.47	0.021	181	29.87
Low	33.74	25.96	0.10	4.22	0.003	98	16.17
Very low	53.38	41.07	0.04	1.69	0.001	44	7.26

Figures

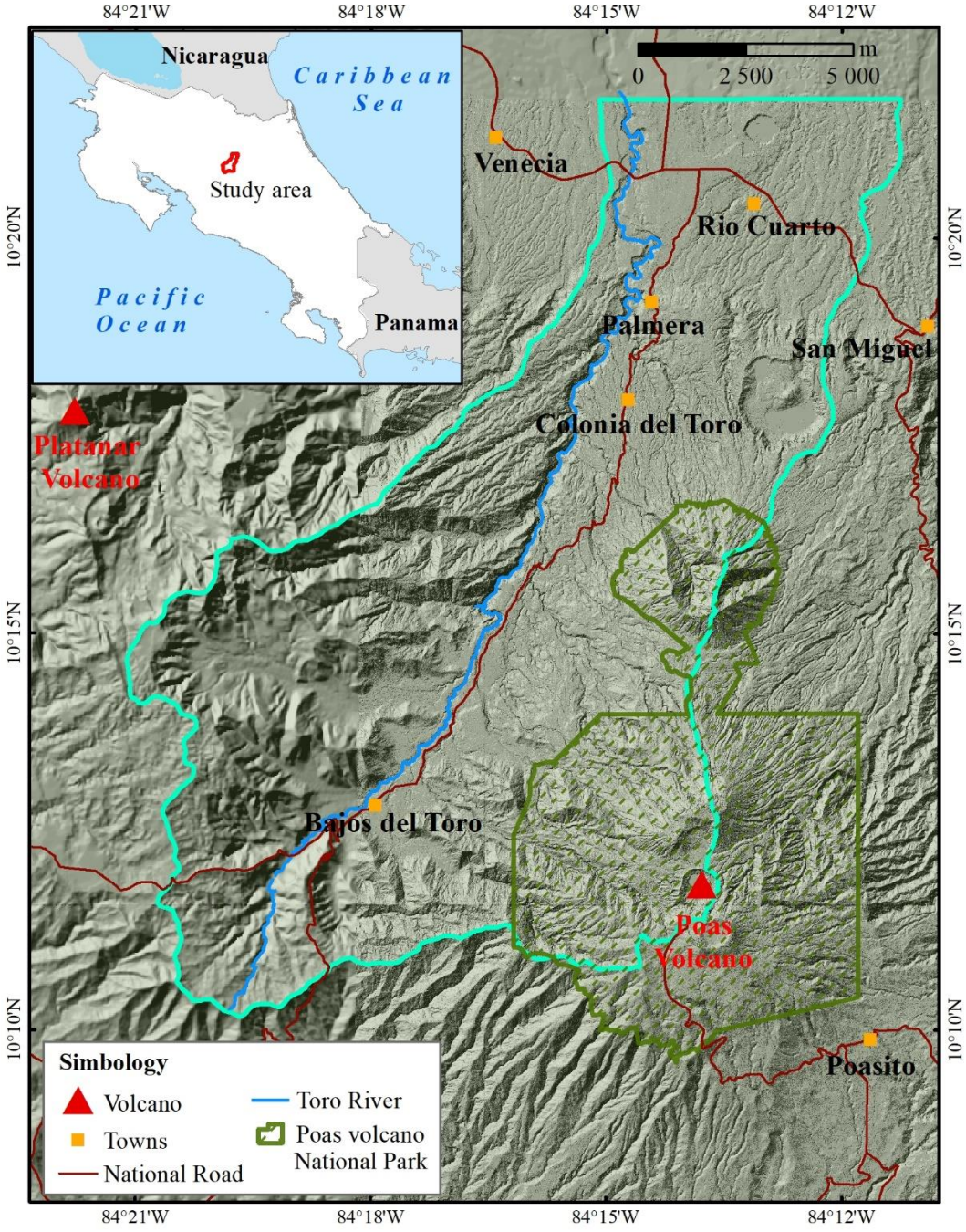

Fig. 1. Map of the study area.

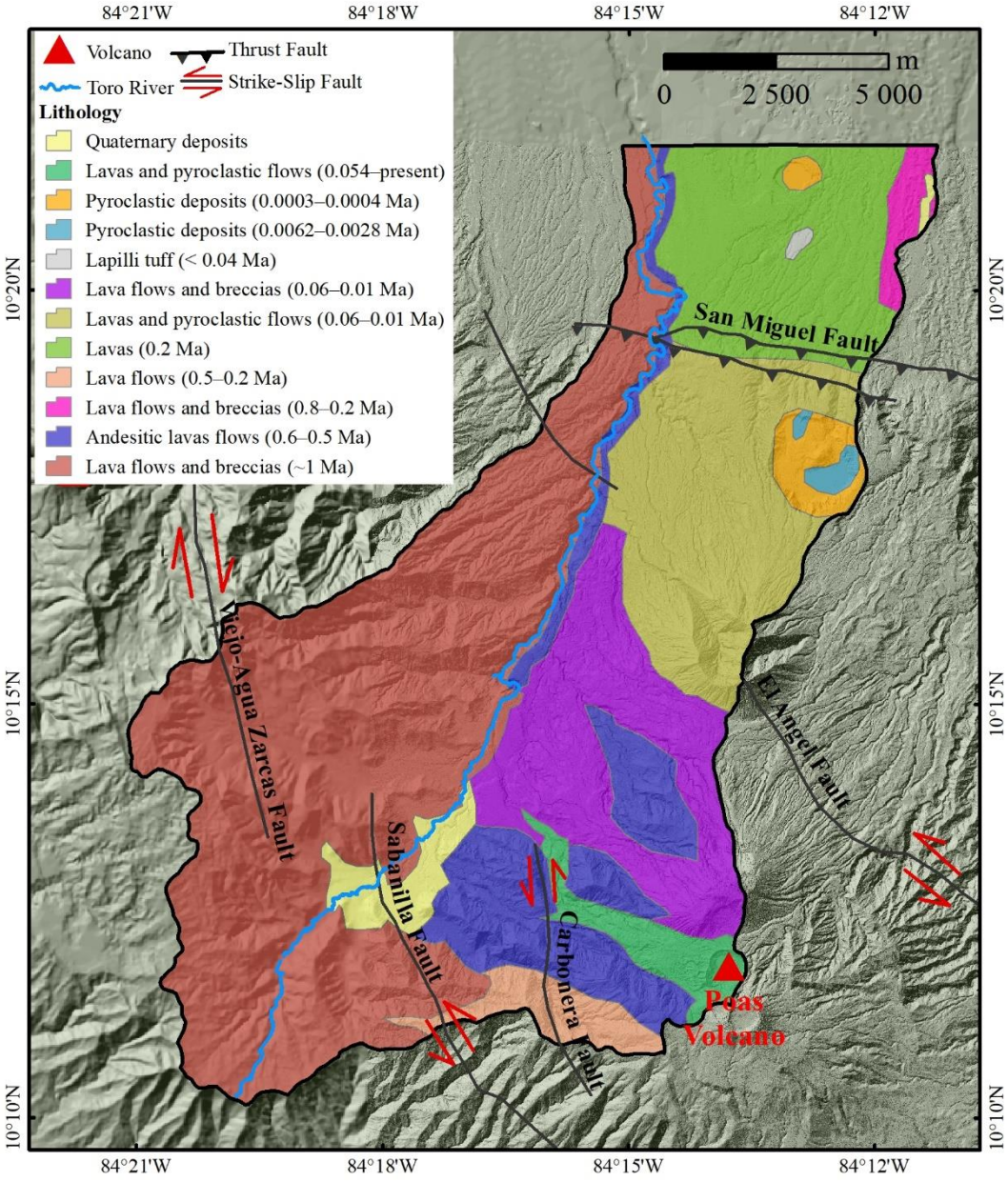

744

745 **Fig. 2**. Geological formations of the study area based on Ruiz et al. (2019a).

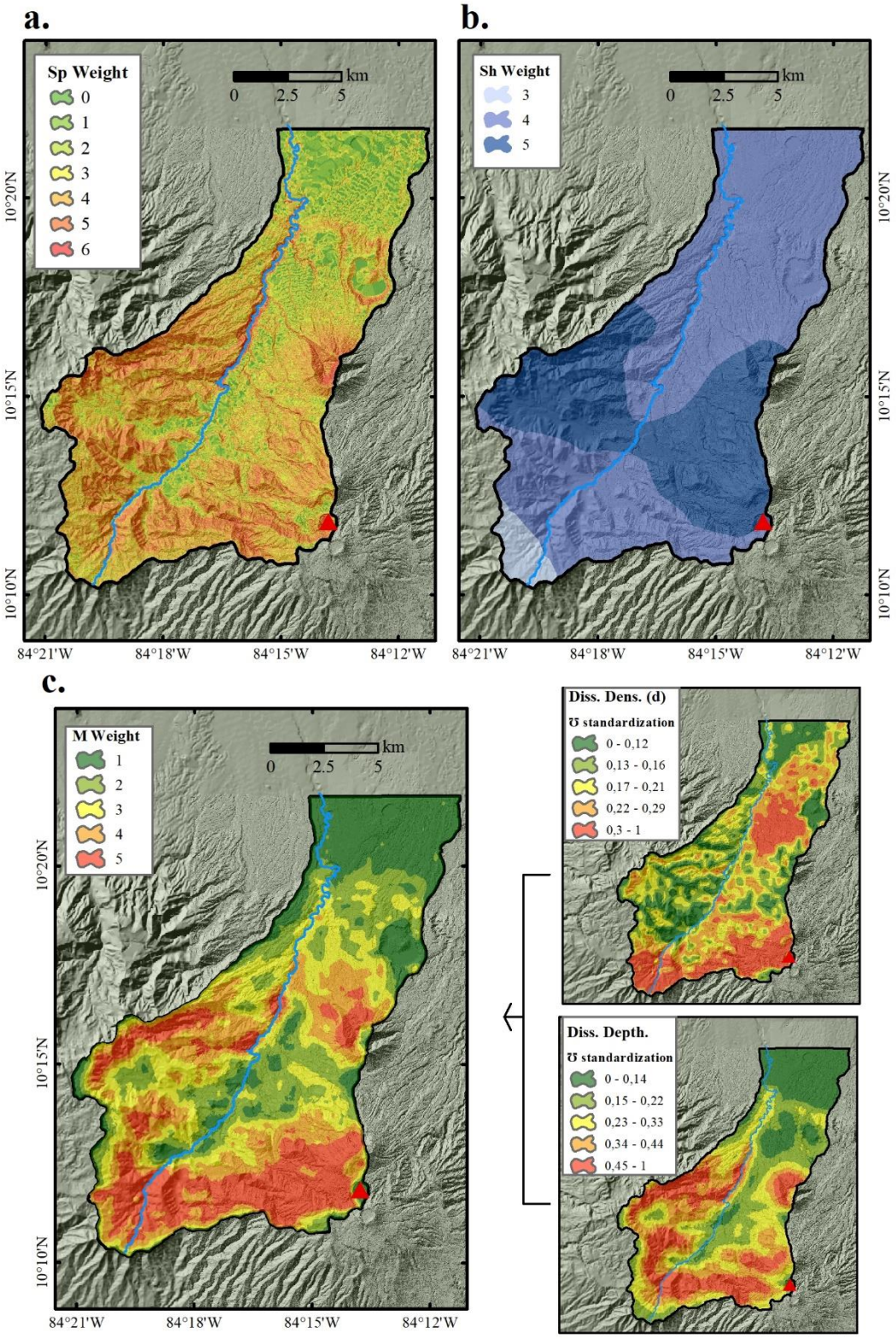

746

747 **Fig. 3**. Control factors considered weighted for landslides susceptibility. a) Slope angle (Sp), b) Humidity content

748 susceptibility (Sh), c) Morphometric susceptibility (M): dissection density + depth density.

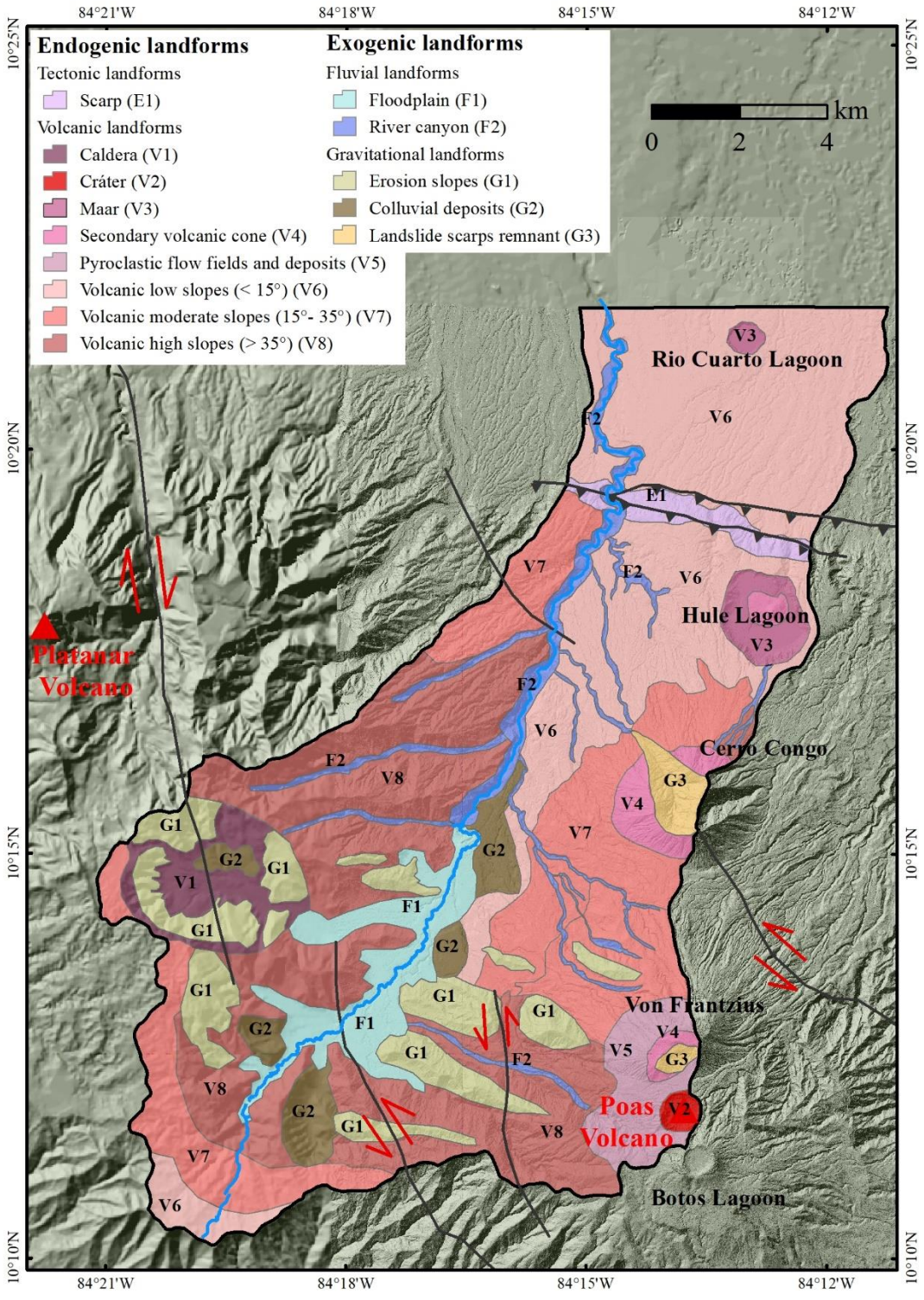

749

750 **Fig. 4**. Geomorphological map and main faults of the NW sector of the Poás volcano. Costa Rica.

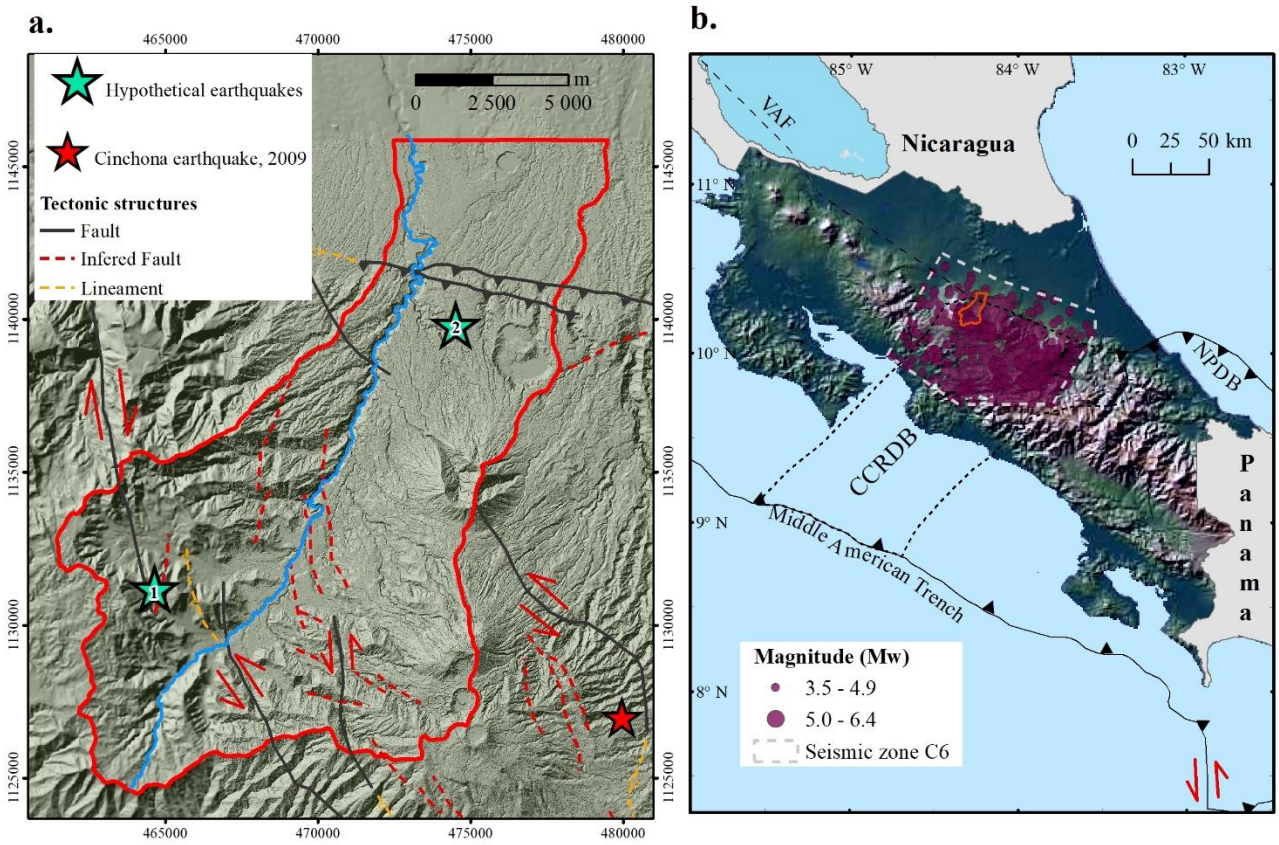

Fig. 5. a) Tectonic framework of the study area and location of the trigger events used (hypotheticals and Cinchona earthquake 2009). 1: Hypothetical earthquake in Viejo-Agua Zarcas Fault. 2: Hypothetical earthquake in San Miguel Fault. The name of the main faults is show in Fig. 2. b) Central Volcanic Cordillera seismic zone and its seismicity between 1723-2018. The region contained within the dotted line represents the Central Costa Rica Deformed Belt (CCRDB). The dashed line represents the simplified northeast boundary of the Central American Forearc Block along the Volcanic Arc Faults (VAF). NPDB is the North Panama Deformed Belt.

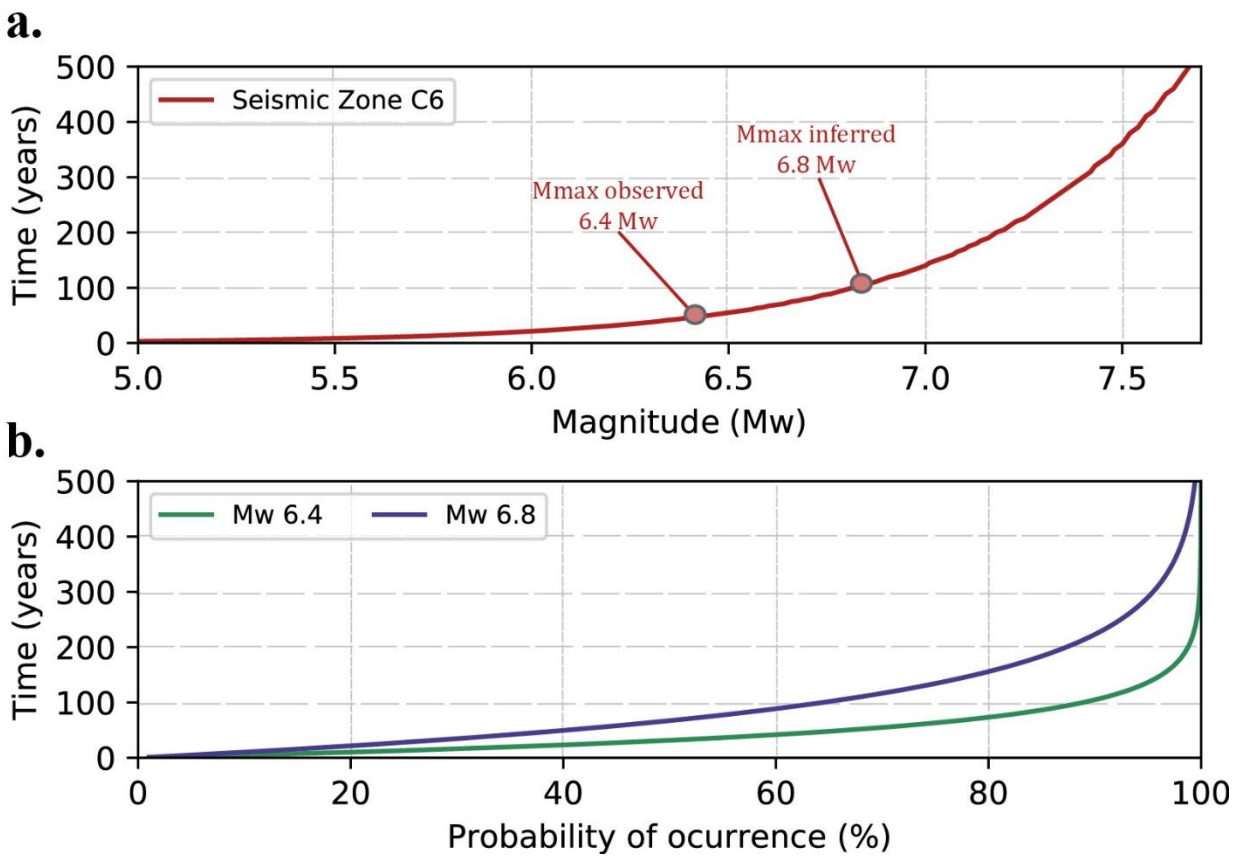

758

759 **Fig. 6**. a) Mean recurrence interval (MRI) for earthquakes of certain Mw for the C6 seismic zone. The Mmax observed

760 and inferred are marked. b) Probability of occurrence (POE) for Mmax observed and inferred in seismic zone C6.

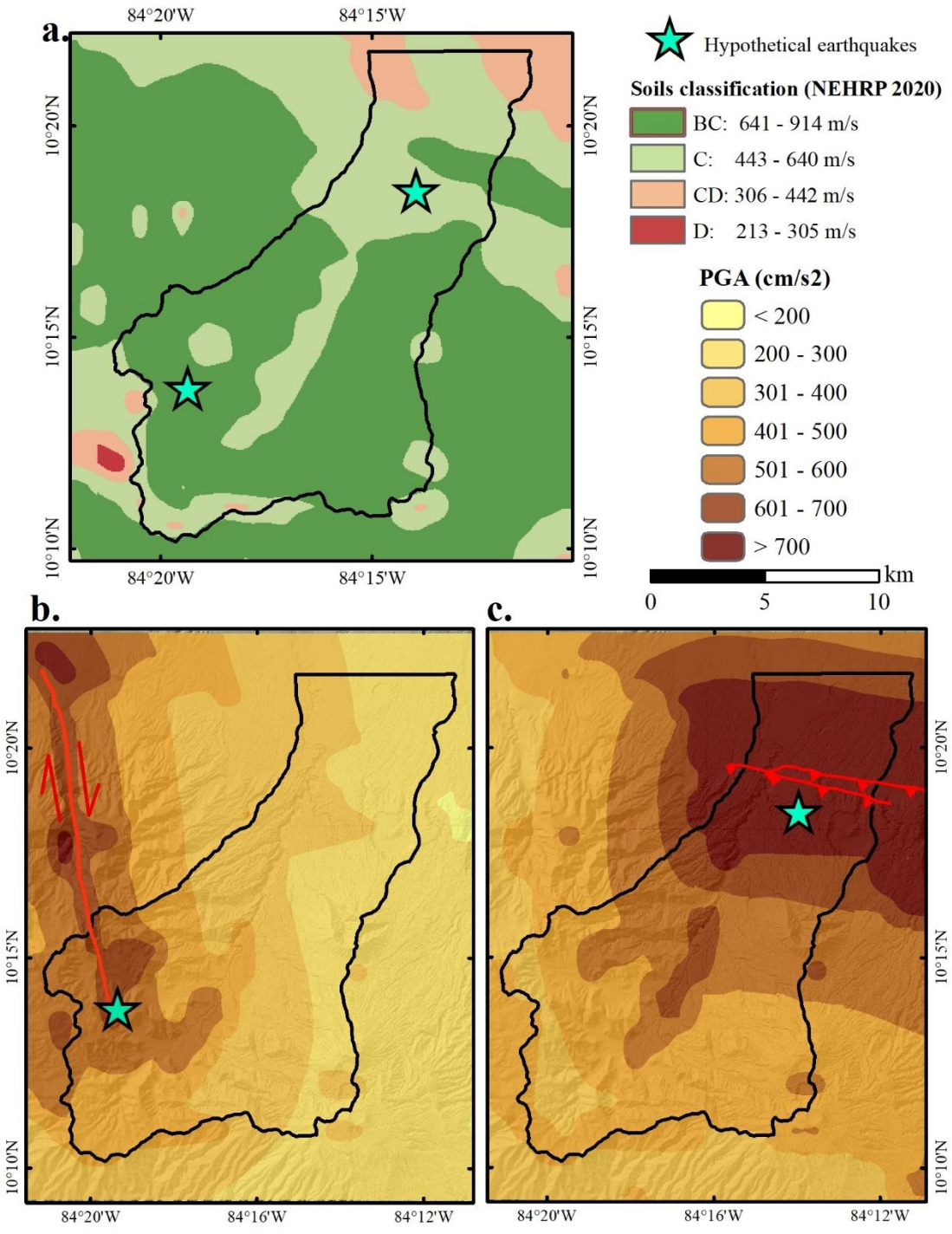

761

762 **Fig. 7.** a) Soils classification and Vs30 values for the study area surroundings, based on topographic slope, with custom

763 embedded maps (NEHRP 2020; Heath et al. 2020). b) Hypothetical earthquake in Viejo-Agua Zarcas strike-slip Fault

764 PGA values (scenario 1). c) Hypothetical earthquake in San Miguel thrust Fault PGA values (scenario 2).

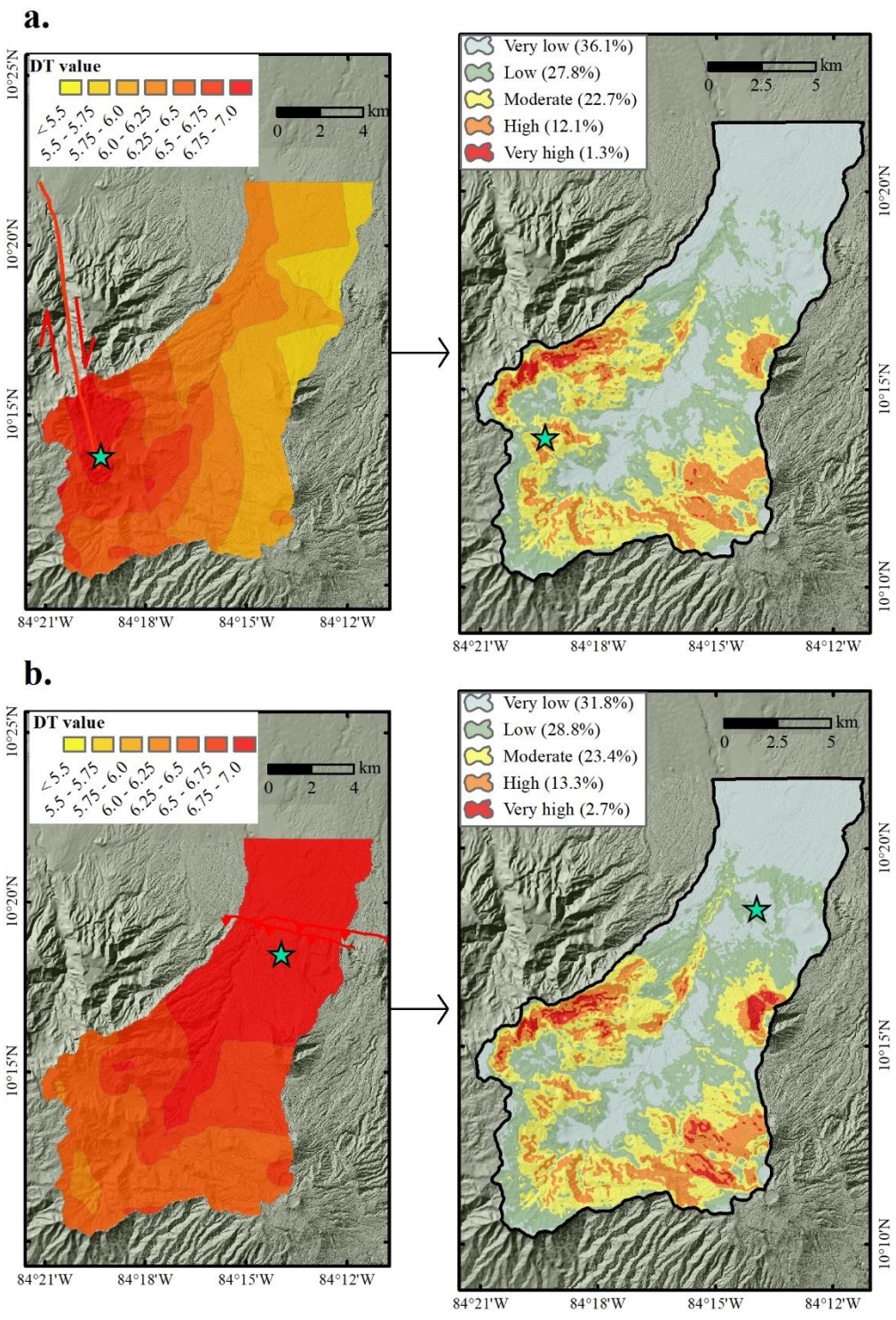

765

766 **Fig. 8.** DT values for hypothetical earthquakes and coseismic landslides susceptibility maps obtained based on its
767 combination with the control factors (Fig 3). a) Trigger event in Viejo-Agua Zarcas strike-slip Fault. b) Trigger event
768 in San Miguel thrust Fault.

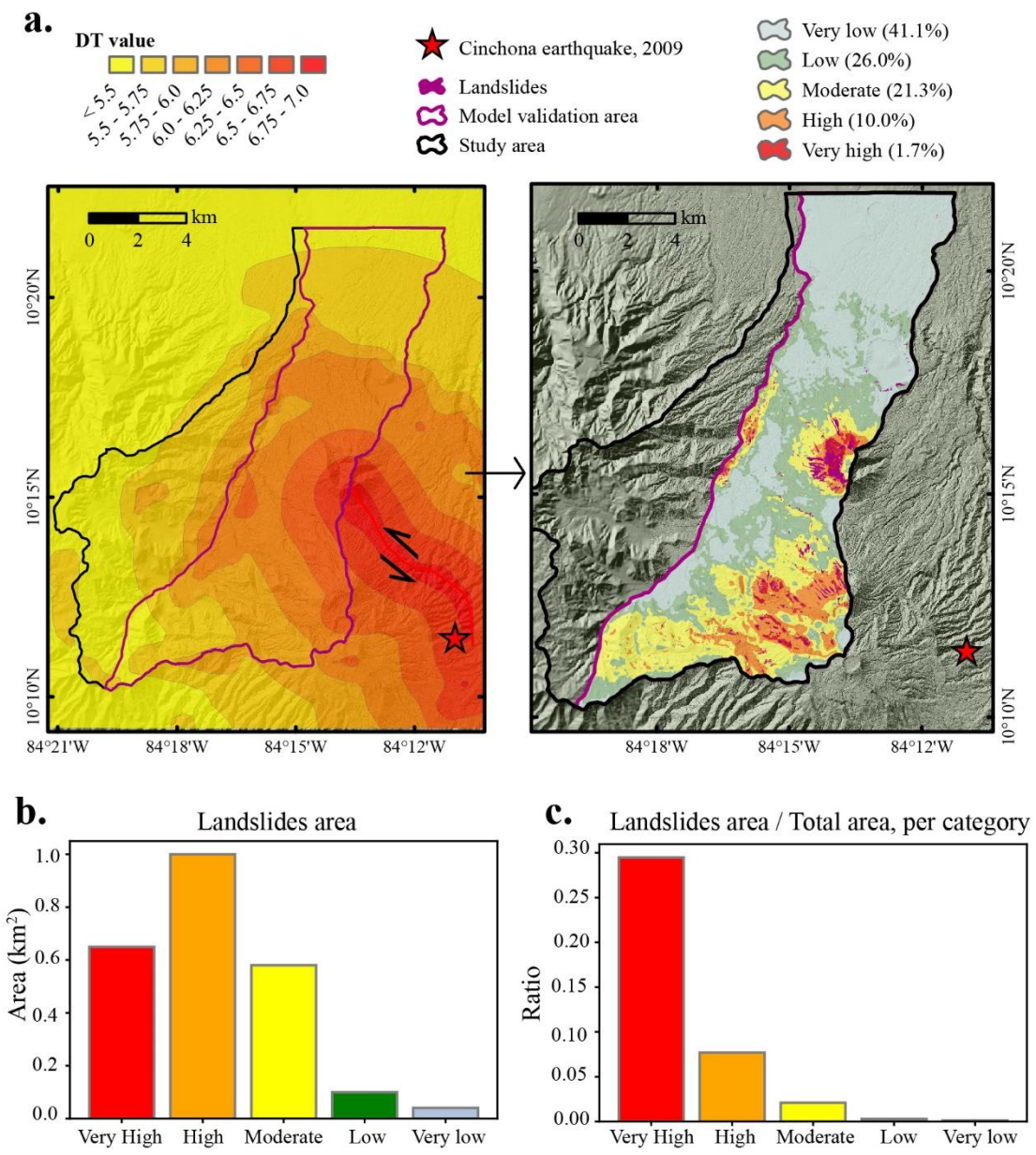

Fig. 9. a) DT values and coseismic landslides susceptibility map for Cinchona earthquake (2009) in the model validation area. b) Area (km^2) from coseismic landslides per susceptibility category. c) Area from landslides per susceptibility category divided by the area covered by each susceptibility category.

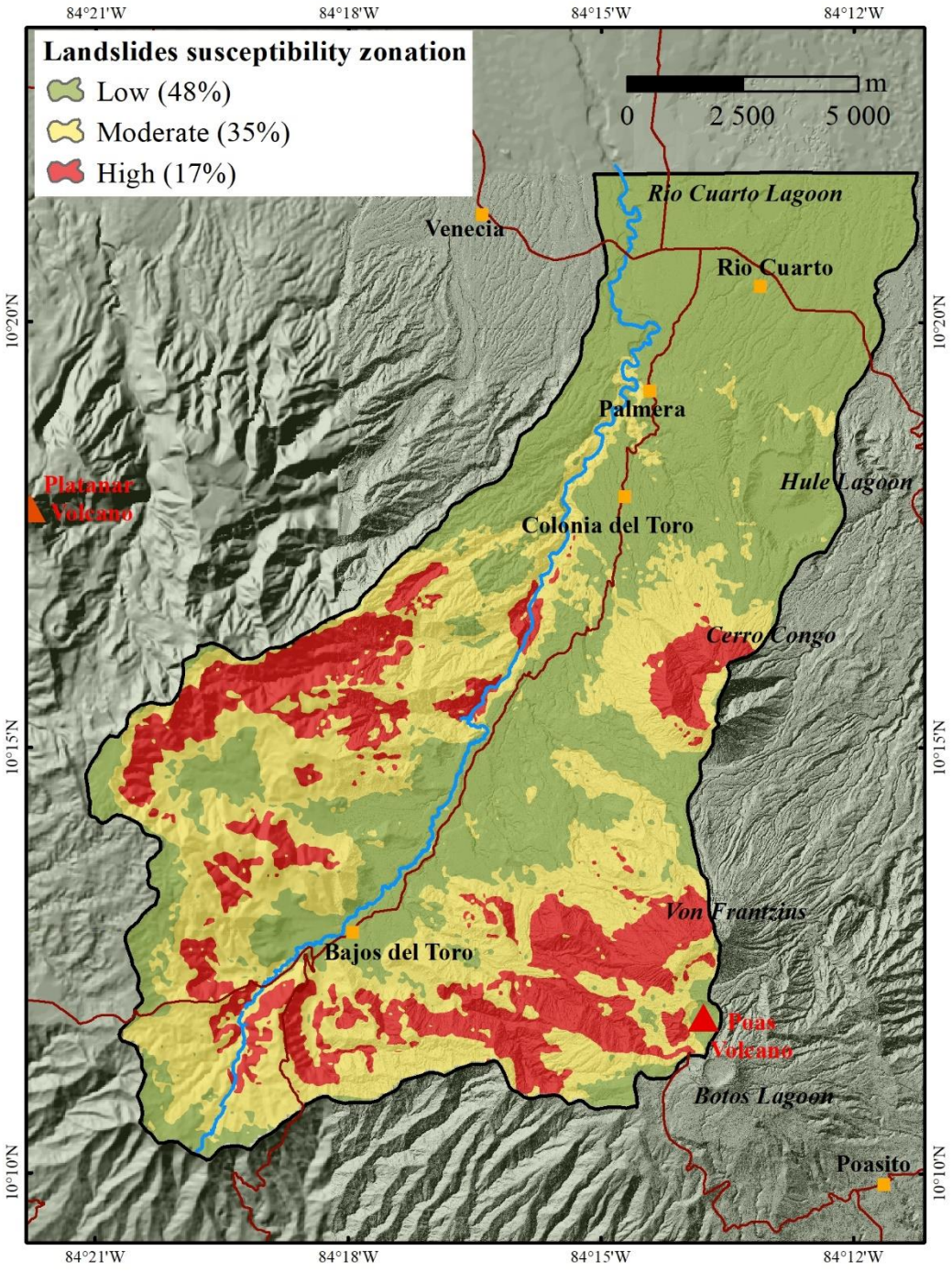

773

774 **Fig. 10**. Zoning of coseismic landslide susceptibility for the NW sector of the Poás Volcano, Costa Rica.